European Journal of Inorganic Chemistry

EurJIC
European Journal of Inorganic Chemistry

Chemistry Europe
European Chemical Societies Publishing

RESEARCH ARTICLE

Synthesis and Magnetism of $Co^{III}_2Co^{II}_5$ and $Co^{III}_2Co^{II}_6$ Complexes, and the Role of the Free Choice of Local Coordinate Frames for Interpreting Magnetic Parameters

Joscha Nehrkorn[1] | Sven Pfirrmann[2] | Yanhua Lan[2] | Christopher E. Anson[2] | Annie K. Powell[2,3,4] | Oliver Waldmann[1]

[1]Physikalisches Institut, Universität Freiburg, Freiburg, Germany | [2]Institute of Inorganic Chemistry, Karlsruhe Institute of Technology, Karlsruhe, Germany | [3]Institute of Nanotechnology, Karlsruhe Institute of Technology, Karlsruhe, Germany | [4]Institute of Quantum Materials and Technologies, Karlsruhe Institute of Technology, Karlsruhe, Germany

Correspondence: Annie K. Powell (annie.powell@kit.edu) | Oliver Waldmann (oliver.waldmann@physik.uni-freiburg.de)

Received: 6 November 2025 | **Revised:** 7 January 2026 | **Accepted:** 8 January 2026

Keywords: cluster compounds | cobalt | exchange anisotropy | magnetic properties | molecular modelling

ABSTRACT

Two new polynuclear high-spin Co^{II} coordination clusters have been synthesised using the proligand *N*-allyldiethanolamine (2,2′-(allylazanediyl)bis(ethan-1-ol), adeaH$_2$). The heptanuclear coordination cluster $[Co^{III}_2Co^{II}_5(adea)_2(\mu_3\text{-}OH)_2(\mu_3\text{-}OMe)_2(\mu_2\text{-}OMe)_2(piv)_6(MeOH)_2]\cdot 2MeOH$ (**1**) possesses a disk-like core motif and was used as a starting material for the syntheses of the octanuclear coordination cluster $[Co^{III}_2Co^{II}_6(adea)_2(\mu_3\text{-}OH)_4(piv)_{10}]\cdot 2Hpiv\cdot 2MeCN$ (**2**). From magnetic measurements a magnetic model could be developed which fits the χT versus T and M versus B curves accurately. In order to rationalise the magnetic properties of **2** it was found essential to consider the consequences of the freedom to choose the local coordinate frames used for describing the individual Co^{II} centres in the cluster. The far-reaching implications of this for the interpretation of magnetic parameters derived from magnetic modelling of clusters containing highly-anisotropic metal ions are discussed.

1 | Introduction

Since the discovery of slow relaxation and quantum tunnelling of the magnetisation in Mn_{12}ac and Fe_8 three decades ago, single-molecule magnets (SMMs) have attracted enormous interest [1–4]. In principle, such systems could be used for data storage [5] or quantum information technology [6–9] on a molecular scale. However, SMMs incorporating only magnetic ions of the 3d row with quenched orbital angular momentum L, such as Mn^{II}, Mn^{III} or Fe^{III}, have been found to be limited in their SMM performance. For instance, SMM behaviour is only observed at very low temperatures (blocking temperatures less than ca 15 K), which represents a major obstacle in using such systems for practical applications [4]. Thus, the search for molecules exhibiting SMM behaviour at higher temperatures has become a major focus of research, with attention shifting toward metal ions with unquenched orbital angular momentum, such as the lanthanides [10–15], since magnetic anisotropy is a key factor in enhancing SMM behaviour [16, 17]. Remarkable progress has indeed been made using lanthanides, with SMM behaviour observed at temperatures above that of liquid nitrogen (77 K) [18]. The best performing lanthanide-based SMMs are however mononuclear complexes (single-ion SMMs), where the high blocking temperatures are achieved owing to their large total angular momentum J and strongly axial anisotropy [19]. Polynuclear lanthanide-based SMMs, in contrast, still exhibit relatively low blocking temperatures, even though, in principle, the anisotropies of the individual ions within the cluster could combine constructively to yield an enhanced overall cluster anisotropy, and, consequently, improved SMM performance. However, this has not yet been realised, which can be attributed to the generally lower symmetry of the ligand coordination environments in these clusters, as well as the weak intramolecular exchange and dipolar magnetic interactions.

Polynuclear Co^{II}-based complexes could appear as interesting candidates in this context. High-spin Co^{II} ions in octahedral environment also exhibit strong single-ion anisotropies due to unquenched angular orbital momenta, but, unlike lanthanides, exchange interactions between them can be strong and promote enhanced cluster anisotropies [20, 21]. Indeed, owing to the favourable properties of the Co^{II} ion, Co^{II}-based SMMs have become a highly active area of research over the past decade, with numerous mono- and polynuclear SMM systems reported in the literature [22–40]. However, modelling and fully understanding the magnetic behaviour of Co^{II} clusters remains a significant challenge [20, 41].

We previously have shown that our synthetic approach to coordination clusters of various combinations of 3d and/or 4f metals [42], in which a combination of *N*-substituted diethanolamine and carboxylate ligands is used, can be successfully applied to prepare a variety of coordination clusters, including pentanuclear cobalt complexes [43]. A useful starting material here is the polymeric Co^{II} pivalate (pivalate = 2,2-dimethylpropanoato) compound $[Co^{II}(piv)_2]_n$, which Winpenny et al. have shown to be a good precursor for cobalt coordination clusters [44–47]. We therefore decided to use this polymeric material in a reaction with *N*-allyldiethanolamine ($adeaH_2$, Scheme 1c). We chose the allyl-substituted diethanolamine ligand with a view towards subsequent ligand functionalization, which is a current focus of further work in this area. However, here we report on the mixed-valent Co^{III}/Co^{II} coordination clusters which can be isolated and characterised structurally, and which we subjected to a detailed study of their magnetic behaviour, which proves to be both fascinating and challenging to understand. The heptanuclear complex $[Co_2^{III}Co_5^{II}(adea)_2(\mu_3\text{-}OH)_2(\mu_3\text{-}OMe)_2(\mu_2\text{-}OMe)_2(piv)_6(MeOH)_2]\cdot 2MeOH$ (**1**, Figure 1a) was isolated from a reaction of the polymeric cobalt pivalate material with the $adeaH_2$ ligand and since it could be obtained in moderately good yield we decided to explore the use of compound **1** as a starting material for further reactions. In particular, reaction of **1** with pivalic acid led to the mixed-valent octanuclear complex, $[Co_2^{III}Co_6^{II}(adea)_2(\mu_3\text{-}OH)_4(piv)_{10}]\cdot 2Hpiv\cdot 2MeCN$ (**2**, Figure 1b) which possesses particularly interesting magnetic properties also described here.

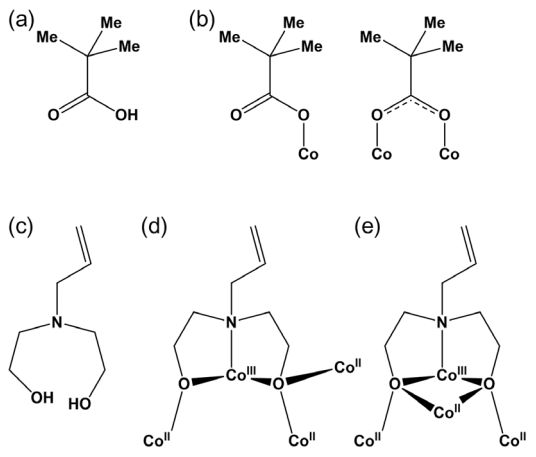

SCHEME 1 | (a) Structure of pivalic acid, (b) coordination modes of pivalate ligands in **1** and **2**, (c) structure of *N*-allyl-diethanolamine ($adeaH_2$), (d) coordination mode of $(adea)^{2-}$ in **1**, (e) coordination mode of $(adea)^{2-}$ in **2**.

For both clusters the magnetic susceptibility and magnetisation curves were recorded, and successfully modelled by using the effective spin-1/2 Hamiltonian approach. There was no evidence for SMM behaviour, as gauged by ac-susceptibility measurements, for either coordination cluster above 1.8 K. However, the magnetic behaviour of cluster **2** proved remarkable in that its magnetism at low temperatures can be described precisely using a strong-exchange model. This is in contrast to the common expectation for Co^{II} clusters, which is that a weak-exchange model should be the appropriate starting point [48]. For the interpretation of this finding we adopted a theoretical framework in which the local coordinate frames used for describing the individual Co^{II} centres in the molecule may be chosen to be different for each centre. The underlying principle is well established in physics and is a standard technique, for example, in the spin-wave theory of magnetic systems with non-collinear spin structures [49–51]. Besides being useful for interpreting the experimental results in **2**, the freedom in choosing the local coordinate frames has also general implications for the magneto-chemical interpretation of the magnetism in polynuclear, exchange-coupled clusters containing magnetic ions with orbitally-degenerate ground states. The identification of this important point is an additional major outcome of this work [52].

2 | Results and Discussion

2.1 | Crystal Structures

Compound **1** crystallizes in the monoclinic space group $P2_1/c$ with $Z = 2$ and its molecular structure is shown in Figure 1. The central cobalt Co(1) is situated on a crystallographic inversion centre. The core of the coordination cluster in **1** consists of seven cobalt ions that are coplanar to within 0.211 Å and form a disk-shaped structure, in which one cobalt lies at the centre of a hexagon formed by the remaining six. The seven metal centres are bridged by six triply-bridging hydroxo or alkoxo ligands that lie alternately above and below the plane. This core topology has been previously reported in cobalt aggregates [48, 53, 54], and is a frequently encountered motif in polynuclear complexes, corresponding to a fragment of a layer within the brucite $M(OH)_2$ structure.

The oxidation states of the cobalt ions were checked using Bond Valence Sum calculations and the calculated values are given in Table 1. Co(4) and its symmetry-equivalent Co(4′) were found to be Co^{III}, while the other five are all Co^{II}. The two $adea^{2-}$ ligands each chelate a Co^{III} centre through their ligand nitrogen and two deprotonated oxygen atoms, O(3) and O(4), which also bridge to three Co^{II} cations. The six triply-bridging groups consist of two methoxo ligands O(1) and O(1′) and two hydroxo ligands O(2) and O(2′), derived from the solvent molecules present, and two alkoxo groups resulting from the deprotonation of oxygens O(3) and O(3′) of the $adea^{2-}$ diethanolamine ligand.

Further bridging around the periphery of the Co_7 disk is provided by two methoxo ligands, with O(5) bridging between Co(4) and Co(3′), and two ligand alkoxo groups, with O(4) bridging between Co(4) and Co(2) plus the respective symmetry equivalents. By contrast, the Co(2)··Co(3) edge (and its symmetry equivalent) has no additional μ_2-alkoxo bridge; instead, this edge is supported by a *syn*,*syn*-carboxylate bridge and by a strong hydrogen bond between the methanol ligand and a unidentate

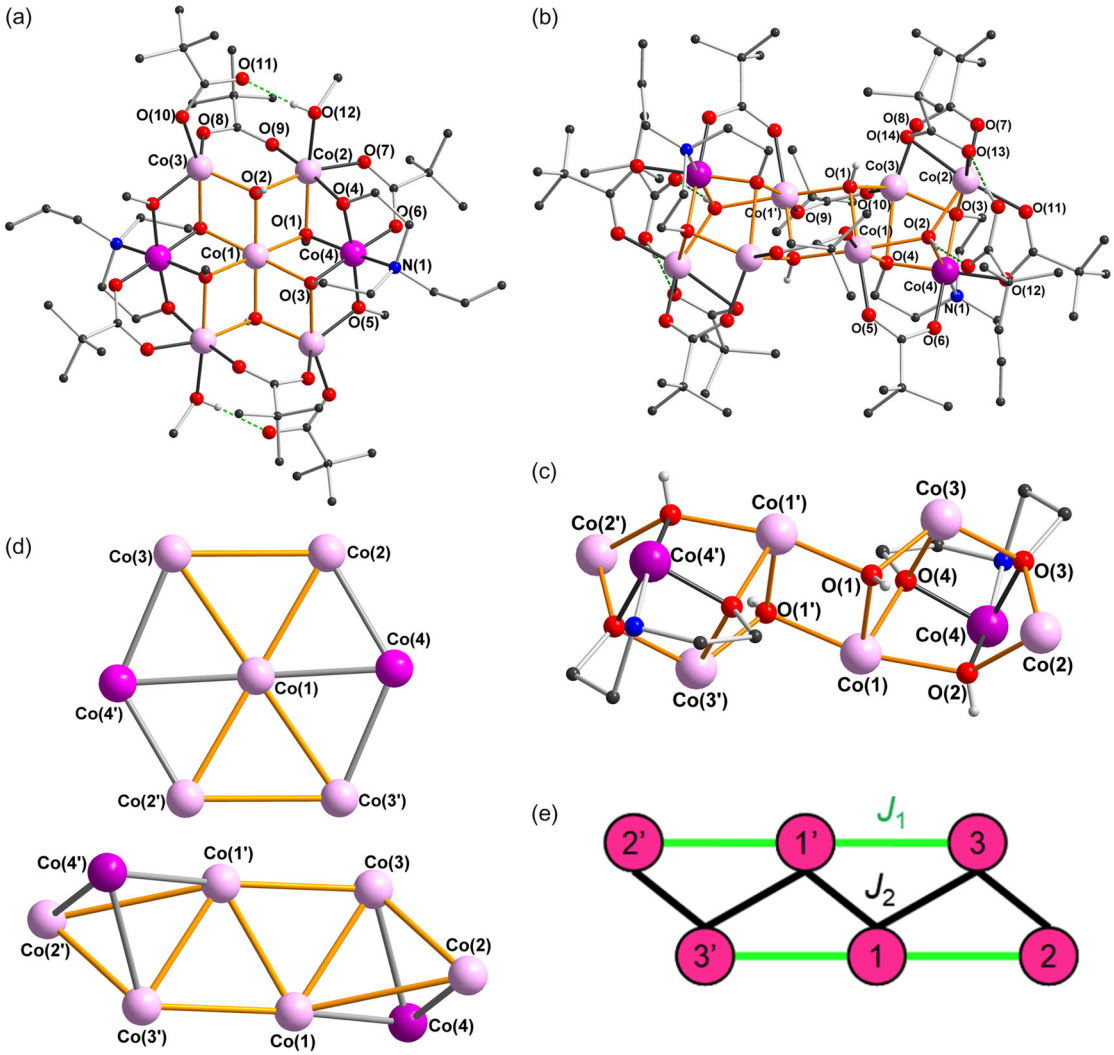

FIGURE 1 | (a) Molecular structure of **1**. Organic H-atoms and minor ligand disorder are omitted for clarity. (b) Molecular structure of **2**. (c) Central core of **2** with allyl groups and pivalates omitted. Co^{III}: purple, Co^{II}: pink, O: red, N: blue, C: dark grey. (d) Metal core topologies of **1** and **2** with Co^{II}-Co^{II} connectivities highlighted in orange. (e) Scheme of the magnetic coupling paths as used in the magnetic models discussed in the text. The labelling of the spin centres follows that in panels (c,d). In the one-*J* model all coupling paths were considered to be equal, while for the two-*J* model the coupling paths along the quasi-linear Co^{II}_3 units (green lines) and those between the members of these units (black lines) were allowed to be different.

carboxylate ligand, with O(11)··O(12) 2.582(3) Å. As a consequence, the Co(2)··Co(3) distance is significantly longer at 3.4525(6) Å than the other Co··Co distances, which fall in the range 2.9562(6)–3.2625(4) Å. Co(1), Co(3) and Co(4) each have distorted octahedral coordination environments, with that of the trivalent Co(4) being as expected less distorted than for the divalent centres as judged by the ranges of X-Co-X angles, while Co(2) is pentacoordinate with a trigonal-bipyramidal geometry, in which O(3′) and O(10) occupy the axial sites.

Since Co(4) and Co(4′) are clearly low-spin Co^{III} and thus diamagnetic, from a magnetic point of view the structure reduces to five Co^{II} ions that form a 'bow-tie' structure [57], in which two triangles share an apex. Examining the Co^{II}-O-Co^{II} bridges between these five centres, the Co(2)-O(2)-Co(3′) (and the corresponding symmetry equivalent) angle of 114.47(10)° is larger than the others, as might be expected given the lack of the extra μ_2-alkoxo bridge between these pairs of cobalts. However, while three of the remaining four independent Co^{II}-O-Co^{II} angles are rather similar, in the range 95.93(7)–96.91(8)°, the fourth, Co(1)-O(2)-Co(2), is significantly more obtuse at 105.85(9)°. This lowering of symmetry is likely to be reflected in the magnetic interactions between the Co^{II} centres.

TABLE 1 | Oxidation states for the Co centres and charges on OH and OMe ligands in **1** and **2** from Bond-Valence Sum Calculations.[a]

	1	**2**
Co(1)	1.97	2.01
Co(2)	2.11	1.94
Co(3)	1.96	1.95
Co(4)	2.97	3.01
O(1)	−1.11	−1.13
O(2)	−1.02	−1.12
O(5)	−0.96	

[a]R_0 values from Wood and Palenik (Co-O) and Brese and O'Keefe (Co-N) [55, 56].

Compound **2** crystallizes in the triclinic space group $P\bar{1}$, with $Z = 1$. The molecular structure of the centrosymmetric octanuclear complex is shown in Figure 1, together with a view of the core of the aggregate. The central part of the core consists of four Co^{II} ions (Co(1) and Co(3) and their inversion counterparts) that describe a planar rhombus, with two $(\mu_3\text{-OH})^-$ ligands (O(1) and O(1′)) each bridging over a triangle of three metals, one above and one below the plane of the rhombus to give the well-known 'butterfly' motif. Two opposite edges of the rhombus, Co(1)··Co(3) and Co(1′)··Co(3′), share an edge of a tetrahedral $Co^{II}_3Co^{III}$ unit. The Co^{III} centre, Co(4), is again chelated by an $adea^{2-}$ ligand in a similar fashion to that in compound **1** (Scheme 1). The two deprotonated oxygens of the ligand, O(3) and O(4), each bridge between Co(4) and two of the Co^{II} centres in the tetrahedron, as does the hydroxo ligand O(2). Three of the four faces of the $Co^{II}_3Co^{III}$ tetrahedron are thus triply-bridged by hydroxo or alkoxo oxygens, and the tetrahedron can thus be considered as a Co_4O_4 cubane in which the oxygen bridging the Co^{II}_3 face is missing.

Around this core, peripheral ligation is provided by ten pivalate ligands, of which two chelate single cobalt centres while the remaining eight form *syn*,*syn*-carboxylate bridges. The two pivalic acid molecules in the crystal lattice are rather strongly hydrogen bonded to the aggregate. Their carboxylic acid groups each form a hydrogen bond to an oxygen O(13) of a chelating pivalate ligand, and also accept a hydrogen bond from the hydroxo ligand O(2).

As in the case of compound **1**, from a magnetic point of view the two Co^{III} ions can be neglected and only a Co^{II}_6 core needs to be considered. In the view of the core in Figure 1c, the Co^{II}-O-Co^{II} bridges have been highlighted in orange. On consideration of the corresponding angles at the oxygen bridges, it becomes apparent that to a first approximation these can be divided into two groups. If the core is regarded as being composed of two parallel, almost linear Co^{II}_3 units, Co(2)··Co(1)··Co(3′) and Co(2′)··Co(1′)··Co(3), then the bridges between metals within these units subtend obtuse angles with Co(1)-O(2)-Co(2) and Co(1)-O(1′)-Co(3′) 131.19(8)° and 112.39(8)°, respectively. The angles corresponding to bridges between the two units are all closer to 90° with Co(1)-O(1)-Co(1′) 97.72(7)°, Co(1)-O(1)-Co(3) 102.54(7)°, Co(1)-O(4)-Co(3) 91.18(6)° and Co(2)-O(3)-Co(3) 93.08(7)°.

It is worth noting that in both **1** and **2** the two $adea^{2-}$ ligands chelate the two Co^{III} centres through their ligand nitrogen and two deprotonated oxygen atoms, while all the Co^{II} ions have six oxygen donors. A similar partition of oxidation states has been noted in other mixed-valence Co^{III}/Co^{II} clusters with diethanolamine ligands [58–60]. The larger ligand field splitting afforded by the nitrogen-containing $adea^{2-}$ ligands apparently favours the stabilisation of low spin d^6 Co^{III}, whereas for the remaining cobalt centres with their six oxygen donors, the high-spin d^7 Co^{II} state is favoured. It is likely that during the formation of **1**, chelation of some of the Co^{II} cations by $adea^{2-}$ ligands facilitates their aerial oxidation to Co^{III}. During the transformation of **1** to **2**, it is likely that the chelated Co^{III} remain in this oxidation state, and that the transformation can be regarded as a substantial structural reorganisation rather than involving any further redox chemistry. In both clusters, the deprotonated oxygens of the $adea^{2-}$ ligands bridge between the chelated Co^{III} and three Co^{II} ions, although the structural motif is more symmetrical in **2** than **1**; the two coordination modes are compared in Scheme 1.

2.2 | Magnetic Characterisation

Magnetic susceptibility studies were performed using both dc and ac fields. No out-of-phase ac-susceptibility signals were observed for either compound. The χT product of cluster **1** (Figure 2a) at 300 K is 14.47 cm^3Kmol^{-1}, i.e., 2.89 cm^3Kmol^{-1} per magnetic ion, which is a common value for a high-spin Co^{II} ion with unquenched orbital angular momentum, but higher than the spin-only value of 1.88 cm^3 $Kmol^{-1}$ expected for a spin 3/2 centre ($g = 2$). With decreasing temperature the χT product decreases continuously from 300 K down to 1.8 K, which in a Co^{II} cluster could be due to crystal-field splitting and/or intramolecular antiferromagnetic couplings. However, the χT product approaches a very small value of 1.04 cm^3 $Kmol^{-1}$ at 1.8 K, which is too low to originate only from the crystal-field effects, indicating the presence of significant antiferromagnetic exchange interactions in the cluster. The field dependence of the magnetisation (Figure 2b) shows a nearly linear increase at 5 K up to the highest available field of 7 T. Some curvature develops at the lower temperatures, but saturation is not reached even at 2 K and fields up to 7 T. At this point the magnetisation assumes a value of 2.93 μ_B, which is much smaller than the saturation moments of about 11 μ_B (5 × 2.2 μ_B) typically expected for a five-membered Co^{II} cluster [35, 43, 53]. This behaviour is another hint regarding the presence of antiferromagnetic couplings in **1**, giving rise to a complicated low-energy spectrum with several levels in the energy range accessible at 2 K in fields up to 7 T.

The temperature dependent χT curve for compound **2** is shown in Figure 3a. At 300 K the χT value is 16.1 cm^3 $Kmol^{-1}$ corresponding to 2.68 cm^3 $Kmol^{-1}$ per Co^{II} centre, which is larger than the spin-only value, again indicating orbital contributions from the Co^{II}

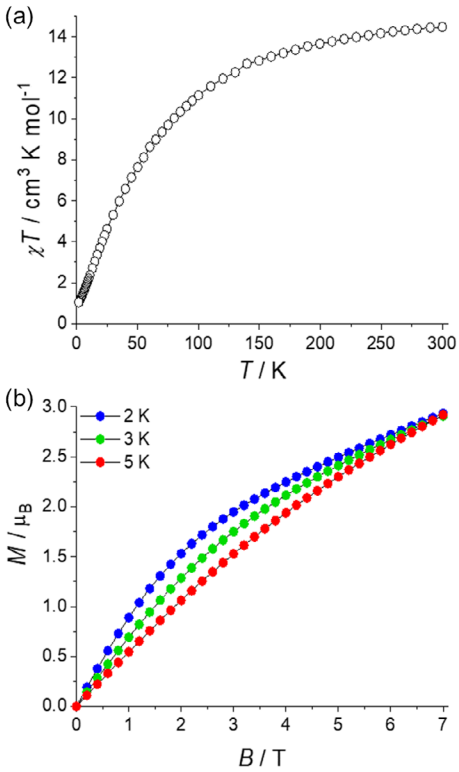

FIGURE 2 | (a) χT versus T curve and (b) magnetisation curves for **1** for the indicated temperatures. The closed and open circles represent the experimental data; the lines are guides to the eye.

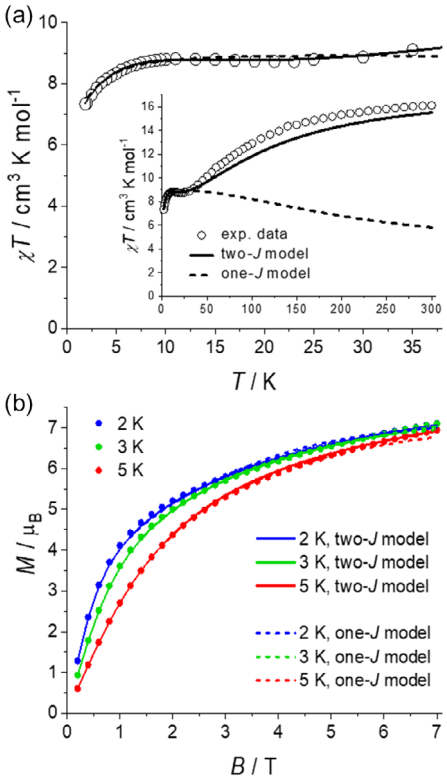

FIGURE 3 | (a) χT versus T curve and (b) magnetisation curves for **2** for the indicated temperatures. The open or closed circles represent the experimental data, the solid and dashed lines represent the simulated best-fit curves for the two-J and one-J models, respectively. The inset to panel (a) shows the χT curve up to the highest measured temperature of 300 K, together with the simulated results for the two-J and one-J models.

ions. The χT product decreases steadily with decreasing temperature, reaching a plateau-like feature at about 10–35 K, with a value of about 8.8 $cm^3\ Kmol^{-1}$. On further decreasing the temperature below 10 K, χT again decreases to reach a value of 7.33 $cm^3\ Kmol^{-1}$ at 1.8 K. The magnetisation curves (Figure 3b) increase linearly at low fields and then show a slower increase without clear saturation even up to 7 T, which is common behaviour for such a Co^{II} cluster. However, at 2 K and 7 T the magnetisation is 7.11 μ_B, which is smaller than the value expected for six uncoupled or ferromagnetically coupled Co^{II} centres, suggesting the presence of antiferromagnetic couplings in the cluster.

At this point it should be stressed that the above discussion regarding the nature of the exchange coupling, in terms of antiferro- or ferromagnetic, is based on the usual 'common sense' arguments regarding the relationship between the thermal evolution of the χT product and type of exchange coupling. However, in Co^{II} clusters (and other clusters containing highly-anisotropic metal ions) such arguments may fail, as we demonstrated for a Co^{II}_5 complex [43]. In fact, a definitive conclusion concerning the nature of the couplings can only be obtained through modelling the data.

2.3 | Analysis

The dc magnetic data were analysed by least-square fitting to an effective spin-1/2 Hamiltonian in order to extract values for the magnetic parameters. Each Co^{II} (d^7) ion is coordinated by six oxygen atoms, resulting in a distorted octahedral environment and a weak (or intermediate, depending on notation) ligand field [20, 61]. Accordingly, a high-spin $S = 3/2$ state is expected. The octahedral component of the ligand field leads to a splitting of the orbital energies on the order of several 1000 K and gives rise to an orbital triplet ground state (which is usuall described by an effective orbital angular momentum $l = 1$). The combined effects of the splittings within the orbital triplet due to distortions from ideal octahedral symmetry and spin–orbit coupling further split the energies into six Kramers doublets with energy separations on the order of 100 K or more. Hence, below about 40 K only the ground-state Kramers doublet is thermally populated, and each Co^{II} centre can be described by an effective spin $s = 1/2$ [20, 41, 62]. The interaction with an external magnetic field $\mathbf{B}$ may be described by a Zeeman-type Hamiltonian $\mu_B \hat{\mathbf{s}}_i \cdot \mathbf{g}_i \cdot \mathbf{B}$, where the index i refers to the i-th Co^{II} centre in the cluster. Typically the g matrices $\mathbf{g}_i$ are highly anisotropic [63]. The exchange interaction between two Co^{II} ions is described by a Hamiltonian of the form $\hat{\mathbf{s}}_i \cdot \mathbf{J}_{ij} \cdot \hat{\mathbf{s}}_j$, where the coupling tensor $\mathbf{J}_{ij}$ allows for both isotropic and anisotropic exchange to be taken into account (antisymmetric exchange shall be neglected here). In principle, a second-order term of the form $-(1/2)\mathbf{B} \cdot \chi_0 \cdot \mathbf{B}$ also appears, which results in a temperature-independent paramagnetism (TIP)-type of contribution. For certain systems this TIP contribution can have significant effects [62] but in the present case of clusters **1** and **2** it can safely be neglected on account of its small relative magnitude. The effective spin Hamiltonian for each of the clusters would, in principle, involve more than a hundred magnetic parameters, which are evidently too many to be determined from our experimental data, hence the necessity to make reasonable approximations and assumptions.

First, uniaxial symmetry was assumed, i.e., all matrices $\mathbf{g}_i$ and $\mathbf{J}_{ij}$ were assumed to be diagonal and each be described by two parameters for the xy and z directions, respectively. Furthermore, the matrices $\mathbf{g}_i$ were assumed to be equal for all ions. Also, not more than two different exchange coupling paths were allowed for. It is noted that, although not necessarily justified from first principles such as molecular symmetry, these sorts of assumptions are frequently made for polynuclear Co^{II} clusters in order to avoid the problem of over-parametrization (with exceptions, e.g., Co^{II} dimers [64]). Finally, as a further provision against over-parametrization, the temperature dependent χT data below 40 K as well as the magnetisation curves at the three different temperatures were simultaneously used within a fit.

For complex **1**, although excellent fits to the measured data could often be obtained, the situation was such that all tested models fell into one of two unhelpful categories. Either no good fit could be obtained at all, or else several excellent fits, involving many different and obviously unrelated parameter sets, were found, but it was not possible to determine which of these was the true one as the fits were all of comparable quality. In other words, the models were either too constrained to allow for a good fit, or over-parametrised and allowing many equally good fits, with little in between. Unfortunately, we encounter this situation quite frequently in the analysis of the magnetic data of Co^{II} complexes, preventing us from obtaining meaningful magnetic parameters. Hence, in conclusion, the experimental data for **1** could be very well reproduced but reasonable values for the magnetic

parameters could not be safely inferred, and thus it is not sensible to make further statements regarding this compound.

In contrast, for complex **2** the attempts at fitting the magnetisation data were successful in the sense that out of the many tested models, two yielded fits that were both good and stable and that converged to unique parameter sets. In the first model, which is the simpler one, all coupling matrices $\mathbf{J}_{ij}$ were taken as equal (the exchange paths in **2** are depicted schematically in Figure 1e). It will hence be referred to as the one-*J* model. Secondly, in the two-*J* model the exchange couplings along the two quasi-linear Co_3^{II} units were allowed to differ from those between the members of the upper and the lower linear units. The Hamiltonian is then as given in Equation (1),

$$\hat{H} = -\sum_{i<j}\left(J_{ij,xy}(\hat{s}_{i,x}\hat{s}_{j,x} + \hat{s}_{i,y}\hat{s}_{j,y}) + J_{ij,z}\hat{s}_{i,z}\hat{s}_{j,z}\right) + \mu_B\sum_i\left(g_{i,xy}(\hat{s}_{i,x}B_x + \hat{s}_{i,y}B_y) + g_{i,z}\hat{s}_{i,z}B_z\right) \quad (1)$$

where the first summation has to be understood as the sum over the exchange pathways depicted in Figure 1e. In the two-*J* model, the Hamiltonian involves the four exchange parameters $J_{1,xy}$, $J_{1,z}$, $J_{2,xy}$ and $J_{2,z}$, and the two *g* factors g_{xy} and g_z.

The one-*J* model is retrieved from this by setting $J_{1,xy} = J_{2,xy} \equiv J_{xy}$ and $J_{1,z} = J_{2,z} \equiv J_z$. However, in this case we have observed that although reasonable best-fit values for the exchange coupling constants were obtained, the estimated standard deviations (esd) were unreasonably large. This could be associated to the fact that in this model the higher-lying energy levels are too high in energy to be reliably determined from the experimental data and resolved by a parameter change from J_{xy} and J_z to the parametrization $J = (2J_{xy} + J_z)/3$ and $D_J = J_z - J_{xy}$. With these, the best-fit parameters were obtained as D_J = 5.56(8) K, J = 270(40) K, g_{xy} = 2.47(1) and g_z = 2.40(1). As can be seen, the value of J is quite large, i.e., larger than the temperature range of up to 40 K accessed in the fits, resulting in a large esd for J. The fits corresponding to the χT and $M(B)$ curves are shown in Figure 3, and reproduce the data below 40 K very well. A similar parametrization issue was not observed for the two-*J* model, which yielded a unique and stable fit with the best-fit parameters $J_{1,xy}$ = −205(6) K, $J_{1,z}$ = 205(7) K, $J_{2,xy}$ = 70(4) K, $J_{2,z}$ = 29(2) K, g_{xy} = 6.67(3), and g_z = 2.37(1). Both the χT curve below 40 K and the $M(B)$ curves are reproduced excellently in this model, as shown in Figure 3. The magnitudes and anisotropies of the exchange coupling constants, as well as the *g* factors, fall within the range expected for six-coordinate Co^{II} clusters [20, 35–37, 39–41].

In the above fits only the χT data up to 40 K were used, in order to account for the fact that the effective spin-1/2 approach becomes valid only at temperatures well below about 100 K. However, although at higher temperatures the effective spin-1/2 approach cannot be expected to provide quantitative agreement, it should be expected to at least reproduce the correct trend in the variation of χT with temperature. Therefore, the χT product was numerically simulated for the whole temperature range up to 300 K for the one-*J* and two-*J* models with the respective best-fit parameters. The results are compared to the experimental behaviour in Figure 3. For the one-*J* model the simulated χT continuously decreases with increasing temperature falling off completely from the experimental data. In contrast, the two-*J* model, although it does not exactly reproduce the experimental data, clearly reproduces the correct trend in the temperature dependence. It appears unlikely that an improvement of the one-*J* model that also takes into account the crystal-field splitting would allow for the simulation of the experimental data at higher temperatures, while for the two-*J* model this appears very likely. Hence, based on this physical argument, the one-*J* model was excluded and the two-*J* model considered as appropriate for **2**.

The simulated low-lying energy spectrum is shown for both the one-*J* and two-*J* models in Figure 4. Both models produce a very similar pattern of the lowest energy states. The main difference is in the higher-excited states, which in the one-*J* model lie well above 40 K, explaining the large esd in J observed in the fitting described earlier. In the two-*J* model the next higher-lying states appear in the range of 35–45 K. It is recalled that for both models the *z* component of the total (effective) spin is a conserved quantity, and that hence the states can be labelled by the magnetic quantum number M_z.

A remarkable aspect of the simulated energy spectrum is its clear 'strong-exchange'-like structure, familiar for typical SMMs such as those containing high spin Mn^{III} ions [4]. The seven lowest levels running from $M_z = -3$ to $M_z = +3$ form a parabola very reminiscent to that of a $S = 3$ ground-state spin multiplet with an easy-axis anisotropy parameter or zero-field splitting (ZFS), respectively. Also, the five next-higher lying levels appear to belong to a $S = 2$ multiplet with an easy-axis ZFS. Thereby, the ZFS splitting is significantly smaller than the energy gap between the $S = 3$ ground and $S = 2$ excited multiplet. All this fits perfectly into a strong-exchange limit picture. In fact, the χT data up to around 10–15 K and the magnetisation curves can very well be simulated by the giant-spin Hamiltonian

$$\hat{H}_S = D_S\left(\hat{S}_z^2 - S(S+1)/3\right) + B_4^0\hat{O}_4^0(S) + \mu_B g\hat{\mathbf{S}}\cdot\mathbf{B} \quad (2)$$

with $S = 3$ and the parameters D_S = 1.88(1) K, B_4^0 = 0.57(2) mK, g = 2.49(1) (the resulting curves coincide essentially with those produced by the one-*J* model in this temperature regime, and are hence not explicitly shown).

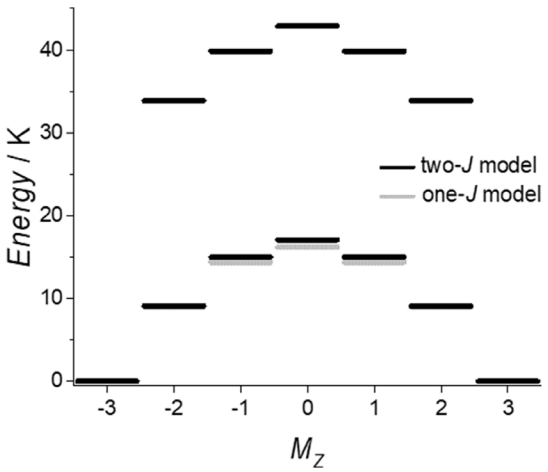

FIGURE 4 | Simulated low-energy part of the zero-field energy spectrum of **2** as function of M_z for the two-*J* (black) and one-*J* (grey) models. The best-fit parameters are given in the text.

However, a strong-exchange limit situation is not obvious from the determined exchange coupling constants in the two-J model, which clearly appear to be very anisotropic. In fact, for the exchange on the two quasi-linear Co_3^{II} units it was found that $J_{1,xy} = -205$ K and $J_{1,z} = +205$ K are essentially equal in magnitude but of opposite sign. This apparent oddity can be understood by noting the freedom to choose the local coordinate frames.

2.4 | Local Coordinate Frames

In this subsection it will be shown how the seemingly strong anisotropy of the exchange interactions in **2** can be reconciled with an energy spectrum and a magnetic low-temperature behaviour which is characteristic for the strong-exchange limit. The invoked considerations point however also to fundamental implications, which will be addressed in the next subsection.

The starting point is the well-known fact that physical observables must not depend on the coordinate frame which is chosen to describe the system. For global coordinate frames (laboratory coordinate frames) the considerations are familiar: A system, which is described in the coordinate frame XYZ by, let's say, the Hamiltonian

$$\hat{H}_{XYZ} = -\sum_{i<j} \hat{\mathbf{s}}_i \cdot \mathbf{J}_{ij} \cdot \hat{\mathbf{s}}_j + \mu_B \sum_i \hat{\mathbf{s}}_i \cdot \mathbf{g}_i \cdot \mathbf{B} \tag{3}$$

can equivalently be described in a different global coordinate frame $X'Y'Z'$, which is obtained from the previous one by a rotation $\mathbf{R}$. In the new frame, the Hamiltonian reads $\hat{H}_{X'Y'Z'} = -\sum_{i<j} \hat{\mathbf{s}}'_i \cdot \mathbf{J}'_{ij} \cdot \hat{\mathbf{s}}'_j + \mu_B \sum_i \hat{\mathbf{s}}'_i \cdot \mathbf{g}''_i \cdot \mathbf{B}'$, where the exchange and g matrices are given by $\mathbf{J}'_{ij} = \mathbf{R}^{-1} \cdot \mathbf{J}_{ij} \cdot \mathbf{R}$ and $\mathbf{g}''_i = \mathbf{R}^{-1} \cdot \mathbf{g}_i \cdot \mathbf{R}$, respectively. The components of the magnetic field in the new coordinate frame $X'Y'Z'$ are calculated as $\mathbf{B}' = \mathbf{R}^{-1} \cdot \mathbf{B}$, and therefore the Zeeman term can also equivalently be written as $\mu_B \sum_i \hat{\mathbf{s}}'_i \cdot \mathbf{g}'_i \cdot \mathbf{B}$ with a g matrix given as $\mathbf{g}'_i = \mathbf{R}^{-1} \cdot \mathbf{g}_i$. We will use this formulation of the Zeeman term in the following.

Importantly, this principle, the free choice of coordinate frame, does not only hold for the global coordinate frame, which applies to the whole molecule as an entity, but also for each of the local coordinate frames $x_i y_i z_i$, which are used to describe the i-th magnetic metal centre. The local coordinate frames are in general not identical, i.e., each magnetic centre i can be described with its own local coordinate frame $x_i y_i z_i$. The statement is then that any physical conclusion does not depend on the choice of the local coordinate frames.

Mathematically, this may be handled as follows (the physical implications will be discussed at the end of the section) [49]: The local coordinate frame $x_i y_i z_i$ of the i-th magnetic centre can be thought of as being generated from a reference frame, which can be chosen without restriction as the XYZ frame, via a rotation matrix $\mathbf{R}_i$, that is, $x_i y_i z_i = \mathbf{R}_i XYZ$. Expressed in the set of local coordinate frames $x_i y_i z_i$ the Hamiltonian $\hat{H}_{XYZ}$ of Equation (3) then reads

$$\hat{H}_{\{x_i y_i z_i\}} = -\sum_{i<j} \hat{\mathbf{s}}'_i \cdot \mathbf{J}'_{ij} \cdot \hat{\mathbf{s}}'_j + \mu_B \sum_i \hat{\mathbf{s}}'_i \cdot \mathbf{g}'_i \cdot \mathbf{B} \tag{4}$$

where the exchange and g matrices are given by

$$\begin{aligned} \mathbf{J}'_{ij} &= \mathbf{R}_i^{-1} \cdot \mathbf{J}_{ij} \cdot \mathbf{R}_j, \\ \mathbf{g}'_i &= \mathbf{R}_i^{-1} \cdot \mathbf{g}_i \end{aligned} \tag{5}$$

It is important to note the differences to the relations for a change of the global coordinate frame, in particular for the exchange coupling matrix: The two rotation matrices to the left and right in $\mathbf{J}'_{ij} = \mathbf{R}_i^{-1} \cdot \mathbf{J}_{ij} \cdot \mathbf{R}_j$ are in general not identical, as they refer to different sites i and j. The transformation formula for the g matrix may also look unfamiliar, but its correctness follows by the same argument as above; it results from combining the two steps of first rotating the Zeeman term to $\hat{\mathbf{s}}'_i \cdot (\mathbf{R}_i^{-1} \cdot \mathbf{g}_i \cdot \mathbf{R}_i) \cdot \mathbf{B}'_i$ and then calculating the magnetic field in the rotated frame $\mathbf{B}'_i = \mathbf{R}_i^{-1} \cdot \mathbf{B}$, which combine to $\hat{\mathbf{s}}'_i \cdot (\mathbf{R}_i^{-1} \cdot \mathbf{g}_i) \cdot \mathbf{B} = \hat{\mathbf{s}}'_i \cdot \mathbf{g}'_i \cdot \mathbf{B}$. The matrices $\mathbf{g}'_i$ and $\mathbf{J}'_{ij}$ then in general do not transform as tensors with respect to local coordinate frame rotations. With respect to global coordinate frame rotations, they however do as physically required (for the g matrices this requires additional conventions to be fulfilled, since only $\mathbf{g} \cdot \mathbf{g}^T$ is in general a tensor but not the g matrix itself [20, 65, 66]; but we assume this to have been take care of). If the local coordinate frames or rotation matrices $\mathbf{R}_i$, respectively, are identical for all centres ($\mathbf{R}_i = \mathbf{R} \,\forall\, i$), then, and only then, the familiar transformation from one global coordinate frame to another mentioned earlier is recovered.

It is also important to note that, although the maths may look similar in places, the local coordinate frames introduced here should not be confused with rotations or coordinate frames which are frequently utilised for parametrising exchange or single-ion anisotropies. For instance, instead of specifying the five independent parameters of a second-order single-ion anisotropy contribution, which can be written as $\hat{\mathbf{s}}_i \cdot \mathbf{D}_i \cdot \hat{\mathbf{s}}_i$, by the tensor $\mathbf{D}_i$ it is often more convenient to choose a parametrization in terms of two parameters D_i and E_i and three Euler angles according to $\mathbf{D}_i = \tilde{\mathbf{R}}_i \cdot \tilde{\mathbf{D}}_i \cdot \tilde{\mathbf{R}}_i^{-1}$, where $\tilde{\mathbf{D}}_i = diag(-D_i/3 + E_i, -D_i/3 - E_i, 2/3D_i)$ and $\tilde{\mathbf{R}}_i$ is the rotation matrix associated to the three Euler angles. Similar parametrization schemes are employed for exchange interactions. These anisotropy-related frames are used to obtain a more convenient parametrization of actual, physical anisotropies which are tilted with respect to a global reference frame. In contrast, 'our' local coordinate frames are not a matter of convenient parametrization, but reflection of an underlying ambiguity in the spin Hamiltonian concept. The underlying origin is in fact a free choice of the basis of the Hilbert space of the spins, which when standard spin bases are used is reflected in the spin Hamiltonian by said local rotations [20, 49].

An immediate consequence of the possibility to choose the local coordinate frames differently and at will is that many Hamiltonians with seemingly very different magnetic parameters can be generated, which however all describe the very same physical reality. For global coordinate frames this ambiguity is familiar: The exchange and g matrices contain different values for the magnetic parameters in the different global coordinate frames, but this source of ambiguity is well recognised and can be handled by, e.g., singling out a specific global coordinate frame (the molecule at hand often suggests a preferred global frame). The free choice of local coordinate frames introduces additional ambiguity, the consequences of which seem to have not widely been realised.

As a most simple example, which will however also be helpful for understanding the situation in **2**, a dimer with an isotropic Heisenberg interaction is considered [66]. The Hamiltonian is written as

$$\begin{aligned}\hat{H}_{\text{dimer}} &= -J\hat{\mathbf{S}}_1 \cdot \hat{\mathbf{S}}_2 + \mu_B g\hat{\mathbf{S}} \cdot \mathbf{B} \\ &= -\hat{\mathbf{S}}_1 \cdot \mathbf{J} \cdot \hat{\mathbf{S}}_2 + \mu_B\left(\hat{\mathbf{S}}_1 \cdot \mathbf{g}_1 \cdot \mathbf{B} + \hat{\mathbf{S}}_2 \cdot \mathbf{g}_2 \cdot \mathbf{B}\right)\end{aligned} \tag{6}$$

with the exchange and g matrices

$$\mathbf{J} = J\begin{pmatrix}1 & 0 & 0\\ 0 & 1 & 0\\ 0 & 0 & 1\end{pmatrix}, \qquad \mathbf{g}_1 = \mathbf{g}_2 = g\begin{pmatrix}1 & 0 & 0\\ 0 & 1 & 0\\ 0 & 0 & 1\end{pmatrix} \tag{7}$$

In writing down these expressions it was implicitly assumed that all local coordinate frames are identical, for instance as in Figure 5a.

Alternatively, however, one could also choose the local coordinate frames shown in Figure 5b, which are obtained via the rotation matrices

$$\mathbf{R}_1 = \begin{pmatrix}1 & 0 & 0\\ 0 & 1 & 0\\ 0 & 0 & 1\end{pmatrix}, \qquad \mathbf{R}_2 = \begin{pmatrix}-1 & 0 & 0\\ 0 & -1 & 0\\ 0 & 0 & 1\end{pmatrix} \tag{8}$$

In this set of local coordinate frames, the exchange and g matrices become

$$\begin{aligned}&\mathbf{J}' = J\begin{pmatrix}-1 & 0 & 0\\ 0 & -1 & 0\\ 0 & 0 & 1\end{pmatrix}, \qquad \mathbf{g}_1' = g\begin{pmatrix}1 & 0 & 0\\ 0 & 1 & 0\\ 0 & 0 & 1\end{pmatrix}, \\ &\mathbf{g}_2' = g\begin{pmatrix}-1 & 0 & 0\\ 0 & -1 & 0\\ 0 & 0 & 1\end{pmatrix}\end{aligned} \tag{9}$$

The Hamiltonian with these exchange and g matrices produces exactly the same physical results as the one with the exchange and g matrices of Equation (7). For instance, the zero-field energy spectrum will be identical, in spite of the fact that the exchange matrix in the second case is not of the Heisenberg type, i.e., does not fulfil $J_x = J_y = J_z$. Also, calculated magnetic susceptibility and magnetisation curves, as well as other observables such as electron paramagnetic resonance or inelastic neutron scattering spectra, respectively, will be identical.

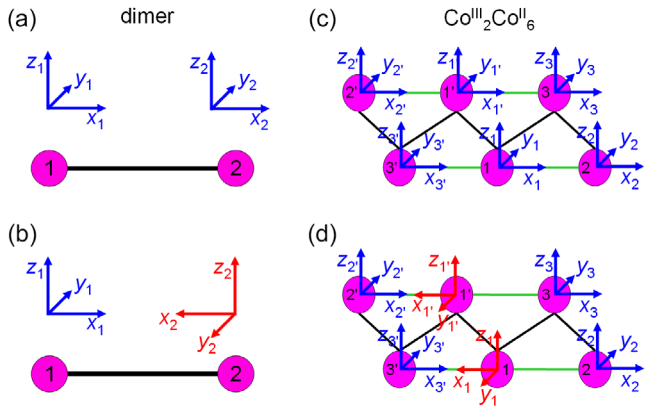

FIGURE 5 | The different sets of local coordinate frames for (a,b) the dimer discussed in the text and for (c,d) the $Co^{III}_2Co^{II}_6$ cluster **2**. In panels (c,d) the labelling of the spin centres is the same as in Figure 1e. The local coordinate frames shown in panels (c,d) correspond, respectively, to the strongly anisotropic and isotropic exchange-coupling situations discussed in the text.

The dimer example suggests the new set of local coordinate frames for the cluster **2** shown in Figure 5d. Here, the local coordinate frames for the Co^{II} centres 1 and 1′ (see also Figure 1) are rotated by the matrix $\mathbf{R}_2$ given in Equation (8). In this representation, sign changes in the xy components of the exchange and g matrices involving centres 1 or 1′ are induced, and the following set of parameters is obtained (esds were omitted for clarity)

$$\mathbf{J}'_{12} = \mathbf{J}'_{13'} = \mathbf{J}'_{1'2'} = \mathbf{J}'_{1'3} = \begin{pmatrix}205\,K & 0 & 0\\ 0 & 205\,K & 0\\ 0 & 0 & 205\,K\end{pmatrix} \tag{10}$$

$$\mathbf{J}'_{23} = \mathbf{J}'_{11'} = \mathbf{J}'_{2'3'} = \begin{pmatrix}70\,K & 0 & 0\\ 0 & 70\,K & 0\\ 0 & 0 & 29\,K\end{pmatrix} \tag{11}$$

$$\mathbf{J}'_{1'3'} = \mathbf{J}'_{13} = \begin{pmatrix}-70\,K & 0 & 0\\ 0 & -70\,K & 0\\ 0 & 0 & 29\,K\end{pmatrix} \tag{12}$$

$$\mathbf{g}'_1 = \mathbf{g}'_{1'} = \begin{pmatrix}-6.67 & 0 & 0\\ 0 & -6.67 & 0\\ 0 & 0 & 2.37\end{pmatrix} \tag{13}$$

$$\mathbf{g}'_2 = \mathbf{g}'_3 = \mathbf{g}'_{2'} = \mathbf{g}'_{3'} = \begin{pmatrix}6.67 & 0 & 0\\ 0 & 6.67 & 0\\ 0 & 0 & 2.37\end{pmatrix} \tag{14}$$

which leads to exactly the same results as shown before for Hamiltonian (1). With these parameters it however becomes immediately obvious that the zero-field energy spectrum and low-temperature magnetisation can be described in the strong-exchange limit: The dominant exchange couplings, which are those along the quasi-linear Co^{II}_3 units and were previously denoted as J_1, are now isotropic and strongly ferromagnetic, immediately explaining a $S = 3$ ground state ($\sum_i s_i = 6 \times 1/2 = 3$). The couplings between the two quasi-linear units, which were denoted before as J_2, are weaker, and anisotropic, leading to an easy-axis ZFS of the $S = 3$ ground multiplet. A proper choice of the local coordinate frames has thus allowed us to rationalise the magnetism in **2**. That is, while the different frames or parameter sets are physically equivalent, they are obviously not for the purposes of interpretation and rationalisation. This is a key result of this work.

It should be noted that the sign change in the xy components of the leading exchange term, which made it essentially isotropic in the new frame (see Equation (10)), is accompanied by a sign change in the xy components of the $\mathbf{g}'_1$ and $\mathbf{g}'_{1'}$ matrices (see Equation (13)). This crucial point will be revisited below.

2.5 | General Implications of the Free Choice of Local Coordinate Frames

The above examples point to intriguing consequences of fundamental importance. They demonstrate that for the components

(eigenvalues) of the exchange-coupling matrix even the type of exchange interaction may change from ferromagnetic to antiferromagnetic. One may thus ask what the notion of 'ferromagnetic' or 'antiferromagnetic' is supposed to mean in highly-anisotropic clusters. We propose here the determinant of the exchange-coupling matrix as criterion. The determinant of the local rotation matrices is $det(\mathbf{R}_i) = 1$ (we only consider proper rotations), and the determinant of the exchange-coupling matrix is thus an invariant, i.e., does not change upon any rotations or local and global frame changes, respectively: $det(\mathbf{R}_i^{-1} \cdot \mathbf{J}_{ij} \cdot \mathbf{R}_j) = det(\mathbf{J}_{ij})$. This can be confirmed explicitly for the specific examples given in the above. In our sign convention, ferromagnetic or antiferromagnetic coupling would then correspond to a positive or negative determinant of the exchange-coupling matrix, respectively.

The two sets of local coordinate frames presented in Figure 5 for cluster **2** are just two examples out of the infinitely many. It is hence clear that, even if one of the local coordinate frames is fixed to coincide with the global coordinate frame, the free choice of local coordinate frames produces infinitely many physically equivalent sets of magnetic parameters. On the other hand, obviously, not all possible sets of magnetic parameters can be physically equivalent and lead to identical magnetic behaviour. However, the physical equivalence of two parameter sets may not necessarily be obvious, as shown by the example of cluster **2**, and therefore the fundamental question arises as of how to detect or categorise the equivalence. In other words, if seemingly very different parameter sets may describe the same physical reality, how then to constructively discriminate against the parameter sets of physically different systems?

Singular value decomposition (SVD) of the exchange matrices can give an answer. SVD allows us to decompose any matrix as $\mathbf{A} = \mathbf{U} \cdot \mathbf{\Sigma} \cdot \mathbf{V}^T$, where $\mathbf{U}$ and $\mathbf{V}$ are orthogonal matrices, $\mathbf{\Sigma}$ is diagonal with the singular values $\sigma_1 \geq \sigma_2 \geq \sigma_3 \geq 0$ on its diagonal, and the singular values are unique [67]. It is then straightforward to show that $\mathbf{J}_{ij}$ and $\mathbf{J}'_{ij} = \mathbf{R}_i^{-1} \cdot \mathbf{J}_{ij} \cdot \mathbf{R}_j$ have identical singular values: From $\mathbf{J}_{ij} = \mathbf{U} \cdot \mathbf{\Sigma} \cdot \mathbf{V}^T$ it follows $\mathbf{J}'_{ij} = \mathbf{U}' \cdot \mathbf{\Sigma} \cdot \mathbf{V}'^T$ with $\mathbf{U}' = \mathbf{R}_i^{-1} \cdot \mathbf{U}$ and $\mathbf{V}'^T = \mathbf{V}^T \cdot \mathbf{R}_j$, and since they both are orthogonal matrices, they establish the SVD for $\mathbf{J}'_{ij}$. Thus, physically equivalent exchange coupling matrices exhibit equal singular values. Two points need to be mentioned. First, in the SVD, the matrices are orthogonal, and it thus can happen that two exchange matrices with equal singular values are related by improper rotations. This is not a problem in principle, since local coordinate frames associated to improper rotations are equally permissible; it may be perceived as inconvenient though. Alternatively, the condition of positive singular values can be lifted, which permits $\mathbf{U}$ and $\mathbf{V}$ to be proper rotations [66]. Second, the topology of the exchange coupling paths can induce constraints. For instance, in a triangle, the transformation of one of the exchange matrices is linked to that of the other two, since with $\mathbf{J}'_{12} = \mathbf{R}_1^{-1} \cdot \mathbf{J}_{12} \cdot \mathbf{R}_2$ and $\mathbf{J}'_{13} = \mathbf{R}_1^{-1} \cdot \mathbf{J}_{13} \cdot \mathbf{R}_3$ the rotations for obtaining $\mathbf{J}'_{23}$ are fixed to $\mathbf{R}_2^{-1}$ and $\mathbf{R}_3$.

The ambiguity induced by the free choice of the local coordinate frame has also implications for attempts to interpret anisotropic exchange interactions in terms of magneto-structural correlation. In light of the above, this is complicated by questions such as which parametrization is to be used or can the exchange parameters inferred for cluster A and cluster B actually be compared. The proposed SVD algorithm in principle provides a methodology to address these concerns, but it is not very intuitive to describe exchange in terms of singular values. Such questions do obviously not occur in the discussion of isotropic or weakly-anisotropic exchange interactions, and meaningful magneto-structural correlations can be established. They do also not occur for the single-ion anisotropy. For instance, in lowest order this anisotropy contribution is described by a term $\sum_i \hat{\mathbf{s}}_i \cdot \mathbf{D}_i \cdot \hat{\mathbf{s}}_i$, which transforms as usual as $\mathbf{D}'_i = \mathbf{R}_i^{-1} \cdot \mathbf{D} \cdot \mathbf{R}_i$ also upon application of local transformations.

Through Equation (6) a link exists between the exchange-coupling matrices and the g matrices; the dimer case and the above results for **2** are explicit examples. If we were able to unambiguously determine the entries in the matrices $\mathbf{g}_i$, then we could unambiguously specify the entries in the exchange-coupling matrices $\mathbf{J}_{ij}$. However, the signs of the principal components (eigenvalues) of a g matrix are not observable, only the sign of its determinant is [20, 65, 66, 68, 69]. As for the exchange matrices, also for the matrices $\mathbf{g}_i$ the determinant is invariant upon local coordinate frame rotations ($det(\mathbf{R}_i^{-1} \cdot \mathbf{g}_i) = det(\mathbf{g}_i)$), which just demonstrates again the physical equivalence exploited in this work. As indicated before, also improper rotations could be used; the discussion would then be somewhat more involved but the conclusion would be the same. The question which of the many parametrization for $\mathbf{J}_{ij}$ to choose cannot be resolved by precise measurements of the g matrices or theoretical ab-initio calculations, but is entirely subject to convention. The point to note is that in highly-anisotropic clusters the exchange-coupling constants themselves are not sufficiently informative, but need to be complemented by information on the g matrices. For materials which contain (only) orbitally-non-degenerate metal ions such an ambiguity in the determination of the exchange-coupling constants does not appear. For these ions the eigenvalues of the g matrices are known to be close to 2 and positive, because of the relatively weak effect of the ligand fields [63]. The ambiguity discussed in this work is an intrinsic aspect of highly-anisotropic metal clusters.

3 | Conclusion

In summary, we have synthesised a $Co_2^{III}Co_5^{II}$ disk-like molecular nanomagnet, which was used as a starting material for the synthesis of another nanomagnetic $Co_2^{III}Co_6^{II}$ cluster. This work has demonstrated that the use of *N*-allyl-diethanolamine together with pivalic acid as co-ligand offers a useful means to obtain high-nuclearity clusters. Additionally, the unsaturated allyl substituent in this ligand opens the potential for subsequent ligand functionalization, e.g., to develop means of depositing the molecules on surfaces. For both clusters we were able to develop a magnetic model which excellently reproduces both the χT versus T curve and the M versus B curves at low temperatures. However, for cluster **1** a unique set of magnetic parameters could not be identified. In contrast, for cluster **2** one reasonable set of magnetic parameters could be determined. To properly understand the magnetic properties in **2** it was found necessary to employ the freedom to choose local coordinate frames at will, which allowed us to understand the strong-exchange characteristics in this compound, which is usually found in weakly-anisotropic systems with a dominant isotropic exchange interaction. Some implications and consequences of this freedom of choice have been discussed. A major consequence is the conclusion that in

clusters which contain highly anisotropic metal ions an unambiguous classification of the eigenvalues of the exchange-coupling tensor as ferromagnetic or antiferromagnetic needs to be linked to a detailed specification of the g matrices for all metal centres in the cluster, which has fundamental implications for any magneto-chemical interpretation of anisotropic exchange interactions.

4 | Experimental

All reactions were performed under aerobic conditions. All chemicals are commercially available and were used without further purification. $[Co(piv)_2]_n$ [47] and *N*-allyldiethanolamine ($adeaH_2$) [70] were synthesised according to the literature procedures.

$[Co^{II}_5Co^{III}_2(adea)_2(OH)_2(OMe)_4(MeOH)_2(piv)_6]\cdot 2MeOH$ (**1**): To a solution of $[Co(piv)_2]_n$ (0.20 g, 0.26 mmol) in MeOH (15 ml) was added $adeaH_2$ (0.028 ml, 0.025 g, 0.17 mmol) and Et_3N (0.2 ml, 0.1451 mg, 1.436 mol). The resulting mixture was stirred for 30 min at 50°C, cooled, filtered to remove any solid and was then allowed to stand undisturbed at room temperature. Dark violet crystals of **1** were formed over 7 days in 0.053 g (13%) yield. Elemental analysis: Calc. (%) for $C_{48}H_{104}Co_7N_2O_{26}$ (corresponding to replacement of each of the methanol ligands and lattice methanols by waters): C 37.47, H 6.82, N 1.82; Found: C 37.57; H 6.66; N 1.81.

$[Co^{II}_6Co^{III}_2(OH)_4(adea)_2(piv)_{10}]\cdot 2Hpiv\cdot 2MeCN$ (**2**): Pivalic acid (0.080 g, 0.78 mmol) was added to a solution of **1** (0.080 g, 0.05 mmol) in a mixture of MeCN (10 ml) and CH_2Cl_2 (5 ml) and stirred for 60 min at 60°C. After filtration, the solution was allowed to stand undisturbed at room temperature with slow evaporation. Dark violet crystals of **2** were obtained after 11 days in 0.065 g (61%) yield. Elemental analysis: Calc. (%) for $C_{74}H_{140}Co_8N_2O_{32}$ (corresponding to the loss of the lattice acetonitriles): C 43.53; H 6.91; N 1.37; Found: C 43.46, H 6.91, N 1.34.

Crystal data for **1**: $C_{52}H_{110}Co_7N_2O_{26}$, 1591.93 g mol^{-1}, monoclinic, $P2_1/c$, T = 100(2) K, a = 15.4660(6), b = 19.1402(8), c = 13.8179(6) Å, β = 115.932(1)°, V = 3678.6(3) Å^3, Z = 2, ρ_{calc} = 1.437 Mg m^{-3}, $F(000)$ = 1666, μ(Mo-$K\alpha$) = 1.610 mm^{-1}; 24 298 data measured, of which 8285 unique (R_{int} = 0.0187); refinement (468 parameters) to wR_2 = 0.1023, S = 1.040 (all data), R_1 = 0.0375 (7021 data with $I > 2\sigma(I)$), largest difference peak/hole = +0.92/−0.41 e Å^{-3}.

Crystal data for **2**: $C_{78}H_{146}Co_8N_4O_{32}$, 2123.43 g mol^{-1}, triclinic, $P\overline{1}$, T = 100(2) K, a = 14.3674(14), b = 14.4878(15), c = 14.9982(15) Å, α = 85.715(2), β = 71.136(2), γ = 61.508(1)°, V = 2584.5(4) Å^3, Z = 1, ρ_{calc} = 1.364 Mg m^{-3}, $F(000)$ = 1114, μ(Mo-$K\alpha$) = 1.323 mm^{-1}; 19 409 data measured, of which 11 194 unique (R_{int} = 0.0175); refinement (661 parameters) to wR_2 = 0.0921, S = 1.050 (all data), R_1 = 0.0388 (9856 data with $I > 2\sigma(I)$), largest difference peak/hole = +0.64/−0.58 e Å^{-3}.

Data were collected at 100 K on a Bruker SMART Apex CCD diffractometer using graphite-monochromated Mo-$K\alpha$ radiation from a rotating anode source and were corrected for absorption using SADABS [71]. The structures were solved using direct methods, followed by full-matrix least-squares refinement against F^2 (all data) using SHELXL [72] within the Olex2 platform [73]. Anisotropic thermal parameters were applied to all non-H atoms. Organic H atoms were placed in calculated positions, while coordinates of H atoms bonded to O were refined. Rigid-bond (RIGU) and geometric (SADI) similarity restraints were applied to the refinement of disordered organic ligands. Full crystallographic data and details of the structural determinations for the structures in this paper have been deposited with the Cambridge Crystallographic Data Centre as supplementary publication nos. CCDC 827 992 and 827 993. Copies of the data can be obtained, free of charge, from https://www.ccdc.cam.ac.uk/structures/.

Magnetic measurements were obtained using a Quantum Design SQUID magnetometer MPMS-XL on freshly-filtered samples. The magnetic data were collected using different techniques of sample mounting such as using a plastic bag as a sample holder and Apiezon grease to restrain the polycrystalline sample to avoid torquing of the molecules. Data were corrected for the sample holder.

Acknowledgments

The authors are grateful for funding by the Deutsche Forschungsgemeinschaft (DFG) through the CFN and the CRC 1573 '4f for Future'.

Open Access funding enabled and organized by Projekt DEAL.

Funding

Deutsche Forschungsgemeinschaft (DFG) (CFN; CRC 1573 "4f for Future").

Conflicts of Interest

The authors declare no conflicts of interest.

Data Availability Statement

Deposition Numbers 827992, 827993 contain the supplementary crystallographic data for this paper. These data are provided free of charge by the joint Cambridge Crystallographic Data Centre and Fachinformationszentrum Karlsruhe Access Structures service. Further data presented in this study are available from the corresponding authors upon reasonable request.

References

1. R. Sessoli, D. Gatteschi, A. Caneschi, and M. A. Novak, "Magnetic Bistability in a Metal-Ion Cluster," *Nature* 365 (1993): 141.

2. R. Sessoli, H. L. Tsai, A. R. Schake, et al., "Strategies Towards Single Molecule Magnets Based on Lanthanide Ions," *Journal of the American Chemical Society* 115 (1993): 1804.

3. G. Christou, D. Gatteschi, D. N. Hendrickson, and R. Sessoli, "Single-Molecule Magnets," *MRS Bulletin* 25 (2000): 66.

4. D. Gatteschi, R. Sessoli, and J. Villain, *Molecular Nanomagnets* (Oxford University Press, 2006).

5. M. Cavallini, J. Gomez-Segura, D. Ruiz-Molina, et al., "Magnetic Information Storage on Polymers by Using Patterned Single-Molecule Magnets," *Angewandte Chemie* 44 (2005): 888.

6. M. N. Leuenberger and D. Loss, "Quantum Computing in Molecular Magnets," *Nature* 410 (2001): 789.

7. M. Affronte, F. Troiani, A. Ghirri, et al., "Single Molecule Magnets for Quantum Computation," *Journal of Physics D: Applied Physics* 40 (2007): 2999.

8. W. Wernsdorfer and M. Ruben, "Synthetic Hilbert Space Engineering of Molecular Qudits: Isotopologue Chemistry," *Advanced Materials* 31 (2019): e1806687.

9. S. Hill, "Making Qubits From Magnetic Molecules," *Physics Today* 78 (2025): 38.

10. N. Ishikawa, M. Sugita, T. Ishikawa, S.-Y. Koshihara, and Y. Kaizu, "Lanthanide Double-Decker Complexes Functioning as Magnets at the Single-Molecular Level," *Journal of the American Chemical Society* 125 (2003): 8694.

11. R. Sessoli and A. K. Powell, "Strategies Towards Single Molecule Magnets Based On Lanthanide Ions," *Coordination Chemistry Reviews* 253 (2009): 2328.

12. L. Sorace, C. Benelli, and D. Gatteschi, "Lanthanides in Molecular Magnetism: Old Tools in a New Field," *Chemical Society Reviews* 40 (2011): 3092.

13. D. N. Woodruff, R. E. P. Winpenny, and R. A. Layfield, "Lanthanide Single-Molecule Magnets," *Chemical Reviews* 113 (2013): 5110.

14. R. A. Layfield and M. Murugesu, *Lanthanides and Actinides in Molecular Magnetism* (Wiley, 2015).

15. S. G. McAdams, A.-M. Ariciu, A. K. Kostopoulos, J. P. Walsh, and F. Tuna, "Molecular Single-Ion Magnets Based on Lanthanides and Actinides: Design Considerations and New Advances in the Context of Quantum Technologies," *Coordination Chemistry Reviews* 346 (2017): 216.

16. O. Waldmann, "A Criterion for the Anisotropy Barrier in Single-Molecule Magnets," *Inorganic Chemistry* 46 (2007): 10035.

17. E. Ruiz, J. Cirera, J. Cano, S. Alvarez, C. Loose, and J. Kortus, "Can Large Magnetic Anisotropy and High Spin Really Coexist?," *Chemical Communications* (England: Cambridge, 2008), 52–54.

18. F.-S. Guo, B. M. Day, Y.-C. Chen, M.-L. Tong, A. Mansikkamäki, and R. A. Layfield, "Magnetic Hysteresis Up to 80 Kelvin in a Dysprosium Metallocene Single-Molecule Magnet," *Science* 362 (2018): 1400.

19. K. Bernot, "Get under the Umbrella: A Comprehensive Gateway for Researchers on Lanthanide-Based Single-Molecule Magnets," *European Journal of Inorganic Chemistry* 26 (2023): e202300336.

20. A. Abragam and B. Bleaney, *Electron Paramagnetic Resonance of Transition Ions* (Oxford: Oxford University Press, 2013).

21. S. Gomez-Coca, E. Cremades, N. Aliaga-Alcalde, and E. Ruiz, "Mononuclear Single-Molecule Magnets: Tailoring The Magnetic Anisotropy Of First-Row Transition-Metal Complexes," *Journal of the American Chemical Society* 135 (2013): 7010.

22. Y.-Y. Zhu, C. Cui, Y.-Q. Zhang, et al., "Zero-Field Slow Magnetic Relaxation From Single Co(II) Ion: A Transition Metal Single-Molecule Magnet With High Anisotropy Barrier," *Chemical Science* 4 (2013): 1802.

23. R. Ruamps, L. J. Batchelor, R. Guillot, et al., "Ising-Type Magnetic Anisotropy and Single Molecule Magnet Behaviour in Mononuclear Trigonal Bipyramidal Co(II) Complexes," *Chemical Science* 5 (2014): 3418.

24. Y.-Y. Zhu, Y.-Q. Zhang, T.-T. Yin, C. Gao, B.-W. Wang, and S. Gao, "A Family of Co(II)Co(III)3 Single-Ion Magnets with Zero-Field Slow Magnetic Relaxation: Fine Tuning of Energy Barrier by Remote Substituent and Counter Cation," *Inorganic Chemistry* 54 (2015): 5475.

25. T. J. Woods, M. F. Ballesteros-Rivas, S. M. Ostrovsky, et al., "Strong Direct Magnetic Coupling in a Dinuclear Co(II) Tetrazine Radical Single-Molecule Magnet," *Chemistry – A European Journal* 21 (2015): 10302.

26. F. Habib, I. Korobkov, and M. Murugesu, "Exposing the Intermolecular Nature of the Second Relaxation Pathway in a Mononuclear Cobalt(II) Single-Molecule Magnet With Positive Anisotropy," *Dalton Transactions* 44(2015): 6368.

27. Y.-Z. Zhang, S. Gómez-Coca, A. J. Brown, M. R. Saber, X. Zhang, and K. R. Dunbar, "Trigonal Antiprismatic Co(II) Single Molecule Magnets With Large Uniaxial Anisotropies: Importance of Raman and Tunneling Mechanisms," *Chemical Science* 7 (2016): 6519.

28. Y. Rechkemmer, F. D. Breitgoff, M. van der Meer, et al., "A Four-Coordinate Cobalt(II) Single-Ion Magnet With Coercivity and a Very High Energy Barrier," *Nature Communications* 7 (2016): 10467.

29. Y. Peng, V. Mereacre, C. E. Anson, et al., "Field-Induced Co(II) Single-Ion Magnets with mer-Directing Ligands but Ambiguous Coordination Geometry," *Inorganic Chemistry* 56 (2017): 6056.

30. X.-N. Yao, J.-Z. Du, Y.-Q. Zhang, et al., "Two-Coordinate Co(II) Imido Complexes as Outstanding Single-Molecule Magnets," *Journal of the American Chemical Society* 139 (2017): 373.

31. F. Shao, B. Cahier, E. Rivière, et al., "Structural Dependence of the Ising-type Magnetic Anisotropy and of the Relaxation Time in Mononuclear Trigonal Bipyramidal Co(II) Single Molecule Magnets," *Inorganic Chemistry* 56 (2017): 1104.

32. S. E. Stavretis, Y. Cheng, L. L. Daemen, et al., "Probing Magnetic Excitations in Co II Single-Molecule Magnets by Inelastic Neutron Scattering," *European Journal of Inorganic Chemistry* 2019 (2019): 1119.

33. S. Nain, M. Kumar, and M. E. Ali, "The Impact of Spin-Vibrational Coupling on Magnetic Relaxation of a Co(II) Single-Molecule Magnet," *Physical Chemistry Chemical Physics* 25 (2023): 14848.

34. H. H. Slavensky, V. S. Parmar, S. S. Leiszner, et al., "Experimental Determination of the Magnetic Anisotropy in Five-Coordinated Co(II) Field-Induced Single Molecule Magnets," *Chemical Science* 16 (2025): 16610–16624.

35. M. Murrie, "Cobalt(II) Single-Molecule Magnets," *Chemical Society Reviews* 39 (2010): 1986.

36. G. E. Kostakis, S. P. Perlepes, V. A. Blatov, D. M. Proserpio, and A. K. Powell, "High-Nuclearity Cobalt Coordination Clusters: Synthetic, Topological and Magnetic Aspects," *Coordination Chemistry Reviews* 256 (2012): 1246.

37. S. Gómez-Coca, D. Aravena, R. Morales, and E. Ruiz, "Large Magnetic Anisotropy in Mononuclear Metal Complexes," *Coordination Chemistry Reviews* 289–290 (2015): 379.

38. A. Sarkar, S. Dey, and G. Rajaraman, "Role of Coordination Number and Geometry in Controlling the Magnetic Anisotropy in FeII, CoII, and NiII Single-Ion Magnets," *Chemistry – A European Journal* 26 (2020): 14036.

39. P. K. Sahu, R. Kharel, S. Shome, S. Goswami, and S. Konar, "Understanding the Unceasing Evolution of Co(II) Based Single-Ion Magnets," *Coordination Chemistry Reviews* 475 (2023): 214871.

40. M. Wang, Z. Han, Y. Garcia, and P. Cheng, "Six-Coordinated CoII Single-Molecule Magnets: Synthetic Strategy, Structure and Magnetic Properties," *ChemPhysChem* 25 (2024): e202400396.

41. A. V. Palii, B. S. Tsukerblat, E. Coronado, J. M. Clemente-Juan, and J. J. Borrás-Almenar, "Orbitally Dependent Magnetic Coupling Between Cobalt(II) Ions: The Problem of the Magnetic Anisotropy," *Journal of Chemical Physics* 118 (2003): 5566.

42. V. Mereacre, A. M. Ako, R. Clérac, et al., "Heterometallic Mn5-Ln4 Single-Molecule Magnets With High Anisotropy Barriers," *Chemistry – A European Journal* 14 (2008): 3577.

43. F. Klöwer, Y. Lan, J. Nehrkorn, O. Waldmann, C. E. Anson, and A. K. Powell, "Modelling the Magnetic Behaviour of Square-Pyramidal Co(II)5 Aggregates: Tuning SMM Behaviour Through Variations in the Ligand Shell," *Chemistry – A European Journal* 15 (2009): 7413.

44. S. J. Langley, M. Helliwell, R. Sessoli, P. Rosa, W. Wernsdorfer, and R. E. P. Winpenny, "Slow Relaxation of Magnetisation in an Octanuclear Cobalt(II) Phosphonate Cage Complex," *Chemical Communications* 40 (2005): 5029–5031.

45. S. Langley, M. Helliwell, R. Sessoli, S. J. Teat, and R. E. P. Winpenny, "Synthesis and Structural and Magnetic

Characterization of Cobalt(II) Phosphonate Cage Compounds," *Inorganic Chemistry* 47 (2008): 497.

46. S. Langley, M. Helliwell, R. Sessoli, S. J. Teat, and R. E. P. Winpenny, "Synthesis and Structural and Magnetic Characterisation of Cobalt(II)-Sodium Phosphonate Cage Compounds," *Dalton Transactions* 16 (2009): 3102–3110.

47. G. Aromí, A. S. Batsanov, P. Christian, et al., "Synthetic and Structural Studies of Cobalt-Pivalate Complexes," *Chemistry – A European Journal*9 (2003): 5142.

48. L. F. Chibotaru, L. Ungur, C. Aronica, H. Elmoll, G. Pilet, and D. Luneau, "Structure, Magnetism, and Theoretical Study of a Mixed-Valence Co(II)3Co(III)4 Heptanuclear Wheel: Lack of SMM Behavior Despite Negative Magnetic Anisotropy," *Journal of the American Chemical Society* 130 (2008): 12445.

49. L. Walker, ed. G. T. Rado and H. Suhl (New York: Academic Press, 1963), 299.

50. O. Cépas and T. Ziman, "Modified Spin-Wave Theory for Nanomagnets: Application to the Keplerate Molecule Mo 72 Fe 30," *Progress of Theoretical Physics Supplement* 159 (2005): 280.

51. O. Waldmann, "E -Band Excitations in the Magnetic Keplerate Molecule Fe_30," *Physical Review B* 46 (2007): 75.

52. J. P. Nehrkorn, "Exploring Molecular Nanomagnets with Spectroscopic Techniques: Spin Exchange Coupling and High Anisotropy, Dissertation," (Dissertation, Universität Freiburg, 2012).

53. K. G. Alley, R. Bircher, O. Waldmann, et al., "Mixed-Valent Cobalt Spin Clusters: A Hexanuclear Complex and a One-Dimensional Coordination Polymer Comprised of Alternating Hepta- And Mononuclear Fragments," *Inorganic Chemistry* 45 (2006): 8950.

54. A. Ferguson, A. Parkin, J. Sanchez-Benitez, K. Kamenev, W. Wernsdorfer, and M. Murrie, "A Mixed-Valence Co_7 Single-Molecule Magnet With C_3 Symmetry," *Chemical Communications* 33 (2007): 3473–3475.

55. N. E. Brese and M. O'Keeffe, "Bond-Valence Parameters for Solids," *Acta Crystallographica Section B Structural Science* 47 (1991): 192.

56. R. M. Wood and G. J. Palenik, "Bond Valence Sums in Coordination Chemistry. A Simple Method for Calculating the Oxidation State of Cobalt in Complexes Containing Only Co-O Bonds," *Inorganic Chemistry* 37 (1998): 4149.

57. S. O. H. Gutschke, D. J. Price, A. K. Powell, and P. T. Wood, "Rational Design of Open-Framework Coordination Solids-Synthesis and Structure of $[Co_5(OH)2\{1,2,4,5\text{-}(O_2C)_4C_6H_2\}2(H_2O)_4]\bullet xH_2O$," *European Journal of Inorganic Chemistry* 2001 (2001): 2739.

58. Y.-W. Li, L.-Y. Guo, L. Feng, Z. Jagličić, S.-Y. Zeng, and S. Di, "Self-Assembly, Structures, Magnetic Properties and Solution Behaviors of Six Mixed-Valence Cobalt Clusters," *CrystEngComm* 19 (2017): 5897.

59. C. Sarto, M. Rouzières, J.-L. Liu, et al., "Slow Magnetization Dynamics in Co(II)/Co(III) Triethanolamine/Pivalate Complexes," *Dalton Transactions* 47 (2018): 17055.

60. S. Schmitz, X. Qiu, M. Glöß, et al., "Conductive Self-Assembled Monolayers of Paramagnetic {CoIICo4III} and {Co4IICo2III} Coordination Clusters on Gold Surfaces," *Frontiers in Chemistry* 7 (2019): 681.

61. C. J. Ballhausen, *Introduction to Ligand Field Theory* (McGraw-Hill: New York, 1962).

62. O. Waldmann, M. Ruben, U. Ziener, P. Müller, and J. M. Lehn, "Supramolecular Co(II)-2 x 2 Grids: Metamagnetic Behavior in a Single Molecule," *Inorganic Chemistry* 45 (2006): 6535.

63. L. F. Chibotaru, A. Ceulemans, and H. Bolvin, "Unique Definition of the Zeeman-Splitting G Tensor of a Kramers Doublet," *Physical Review Letters* 101 (2008): 033003.

64. A. B. Boeer, A.-L. Barra, L. F. Chibotaru, et al., "A Spectroscopic Investigation of Magnetic Exchange Between Highly Anisotropic Spin Centers," *Angewandte Chemie* 50 (2011): 4007.

65. M. H. L. Pryce, "Sign of g in Magnetic Resonance, and the Sign of the Quadrupole Moment of Np237," *Physical Review Letters* 3 (1959): 375.

66. P. J. Alonso and J. I. Martínez, "Magnetic Properties of a Kramers Doublet. An Univocal Bridge Between Experimental Results And Theoretical Predictions," *Journal of Magnetic Resonance*, 255 (2015): 1.

67. G. H. Golub and C. F. Van Loan, *Matrix Computations*. 4th ed. Baltimore, MD: (Johns Hopkins University Press, 2013).

68. L. F. Chibotaru and L. Ungur, "Ab Initio Calculation of Anisotropic Magnetic Properties of Complexes. I. Unique Definition of Pseudospin Hamiltonians and Their Derivation," *Journal of Chemical Physics* 137 (2012): 064112.

69. Y. Pavlyukh, W. Hübner, and G. Lefkidis, "Covariant Approach to Magnetic Anisotropy," *Physical Review B* 100 (2019): 054444.

70. R. W. Saalfrank, C. Deutscher, S. Sperner, et al., "Six-Membered Metalla-Coronands. Synthesis and Crystal Packing: Columns, Compartments, and 3D-Networks," *Inorganic Chemistry* 43 (2004): 4372.

71. G. M. Sheldrick, *SADABS: Program for Empirical Absorption Correction of Area Detector Data* (Göttingen: University of Göttingen, 2006), version 2006/4.

72. G. M. Sheldrick, "Crystal Structure Refinement with SHELXL," *Acta Crystallographica C* 71 (2015): 3.

73. O. V. Dolomanov, L. J. Bourhis, R. J. Gildea, J. A. K. Howard, and H. Puschmann, "OLEX2 : A Complete Structure Solution, Refinement and Analysis Program," *Journal of Applied Crystallography* 42 (2009): 339.